Green hydrogen production: Process design and capacity expansion integrating economic and operational autonomy objectives

Andrés I. Cárdenas[a], Felipe Díaz-Alvarado[a], Ana I. Torres[b]

[a]*Department of Chemical Engineering, Biotechnology, and Materials, Faculty of Physical and Mathematical Sciences, Universidad de Chile, Av. Beauchef 851, Piso 6-poniente, Center for Sustainable Design and Process Systems Engineering, Santiago, 8370456, Metropolitan Region, Chile*
[b]*Department of Chemical Engineering, Carnegie Mellon University, Doherty Hall 5000 Forbes Avenue, Pittsburgh, PA 15213, Pennsylvania, USA*

Abstract

Green hydrogen is an attractive energy vector due to its zero carbon emission in production and use, supporting many industries in their transition to cleaner operations. However, the production of green hydrogen has a fundamental challenge in resilience since it requires renewable energy (RE) systems that are subject to variability. This study develops an optimization-based decision-making framework for the design and capacity expansion of hydrogen production systems at a regional level. A novel resilience objective function that considers external RE-derived fluctuations, as well as internal plant failures, is proposed. An illustrative case study using data from five regions in Chile verifies that consideration of resiliency in the objective function results in a system that is able to overcome the variance without greatly increasing the equilibrium cost for hydrogen. These designs are based on dual storage capacities with different expansion profiles.

Keywords: Green hydrogen, Hybrid Renewable Energy Systems, Dual Storage Systems, Optimal process design, Capacity expansion, Resilience

1. Introduction

Fossil fuels and their greenhouse gas emissions have considerably impacted the environment, specifically on climate change [1]. Renewable energies (REs) are proposed to mitigate this problem; however, REs present new technical challenges compared to traditional fossil resources. For example, renewable sources are susceptible to exogenous effects such as weather conditions, making some of them unpredictable (e.g., tidal and wind energy). As a consequence, the supply has to deal with uncertainty [2].

The concept of a Hybrid Renewable Energy System (HRES) has been developed to withstand this deficiency. It proposes that a system composed of coupled RE sources can complement each other's weaknesses and produce a more stable energy output. In addition, these systems consider various types of energy storage technologies to further improve the desired stability [3].

Green hydrogen has been studied extensively as an energy carrier with no direct carbon emissions during the production phase [4]. This attractive property has led to international interest in developing hydrogen production based on hybrid renewable energy systems. However, dealing with the variability of RE sources is still a pending question in the regional or national-scale HRES design phase.

Research gap exists regarding the use of resilience metrics in the design and optimization of long-term HRES [5]. This paper proposes a metric that provides a quantitative approach to HRES resilience for green hydrogen production by considering the resource variability and the intrinsic failure rate of physical components in the system. This quantitative approach is expressed as an objective function in an optimization problem model to decide the capacity expansion of an off-grid regional-scale green hydrogen production system.

1.1. State of the art: HRES modeling and applications

Mathematical programming has been recently used in power systems and HRES design. For example, Siddaiah and Saini [6] proposes mathematical programming to achieve a specified goal (such as minimal cost or emissions) in HRES design while considering pertinent constraints associated with the system and its parts; Lara et al. [7] proposed a deterministic multi-scale formulation for electric power infrastructure planning, considering annual generation, investment, and hourly operational decisions; Alraddadi et al. [8] modeled the expansion planning of power systems that incorporate a high solar power share, where higher generation and storage capacity is required to meet demand at night; Wang et al. [9] coupled the optimization of a regionally integrated energy system together with eleven sustainability indices to a case study in Xinjiang, China; and Cho et al. [10] implemented a GDP and bilevel decomposition approach for reliable power system planning, determining long-term investment and short-term operational decisions.

Nomenclature

Indexes

d Representative day

e Renewable energy source

i Technology (superstructure equipment)

r Location

t Time of day

Parameters

ΔH Hydrogen electrolysis reaction enthalpy

η^{PV} Solar panel efficiency

η_{Charge} Battery charge efficiency

$\eta_{Discharge}$ Battery discharge efficiency

η_{Tank} Hydrogen tank discharge efficiency

λ Wind turbine swipe area to Land usage ratio

Λ_i Availability of technology i

ρ_{Air} Air density

A_r^{Max} Maximum available area in location r

C_i^{Imlp} Implementation cost of technology i

C_i^{Op} O&M cost of technology i

C_p^{Wind} Wind turbine capacity factor

$Demand_d$ Hydrogen demand for day d (trimester demand)

$G_{t,d,r}^{Sun}$ Average solar radiation at time t at day d in location r

HTL_{Max} Maximum hydrogen level in the hydrogen tank system

$k_{Compressor}$ Compressors power consumption constant

$L^{Battery}$ Battery passive losses

M A sufficiently large number

$P_{H_2}^{Sale}$ Hydrogen selling price

$SOC_{Min,Max}$ Minimal and maximal states of charge for the battery system

η_{AE} Alkaline electrolyzer efficiency

Supplementary definitions

${}^{ext}\Delta E^-{}_{t,d,r}$ Net energy variability from external influences at time t at day d in location r

${}^{ext}\delta E^-{}_{t,d,r}$ Overall energy variability from external influences at time t at day d in location r

${}^{int}\Delta E^-{}_{t,d,r}$ Net energy variability from internal influences at time t at day d in location r

${}^{int}\delta E^-{}_{t,d,r}$ Overall energy variability from internal influences at time t at day d in location r

${}^{int}\Delta M^-{}_{t,d,r}$ Net mass variability from internal influences at time t at day d in location r

${}^{int}\delta M^-{}_{t,d,r}$ Overall mass variability from internal influences at time t at day d in location r

$CAPEX_d$ Implementation cost at day d

DF_d Discount factor at day d

$Land$ Total Land acquisition cost

$OPEX_d$ Operational cost at day d

$Storage_{t,d,r}$ available storage at time t at day d in location r

$\dot{Var}_{e,t,d,r}$ Installed variability associated with source e at time t at day d in location r

$C_{Op\,d}^{H_2}$ Stored hydrogen opportunity cost at day d

Variables

$\dot{E}_{e,t,d,r}^{Direct}$ Energy flow directed to the AE from source e at time t at day d in location r

$\dot{E}_{e,t,d,r}^{Storage}$ Energy flow directed to the battery storage from source e at time t at day d in location r

$\dot{m}_{t,d,r}^{d}$ Mass flows supplied to demand directly from the AE at time t at day d in location r

$\dot{m}_{t,d,r}^{out}$ Outgoing mass flow from the AE at time t at day d in location r

$A_{d,r}^{PV}$ Installed pv panel area at day d in location r

$A_{d,r}^{Wind}$ Installed wind turbine swipe area at day d in location r

A_r Bought Land in location r

$Cap_{i,d,r}$ Capacity of technology i at day d in location r

$CapD_{i,d,r}$ Amount of capacity downgrade for technology i at day d in location r

$CapE_{i,d,r}$ Amount of capacity expansion for technology i at day d in location r

H_r 1 if location r is used in the regional production

$Power_{t,d,r}^{Comp}$ Compressor power consumption at time t at day d in location r

$X_{i,d,r}$ 1 if a decrease for technology i starts at day d in location r

$Y_{i,d,r}$ 1 if an expansion for technology i starts at day d in location r

$\dot{E}_{AE}{}^{in}{}_{t,d,r}$ Total energy flow entering the AE at time t at day d in location r

$\dot{E}_s{}^{in}{}_{t,d,r}$ Energy flow directed to battery storage at time t at day d in location r

$\dot{E}_s{}^{out}{}_{t,d,r}$ Energy flow directed to the AE from the battery storage at time t at day d in location r

$\dot{m}_s{}^{in}{}_{t,d,r}$ Mass flow supplied to the hydrogen tank at time t at day d in location r

$\dot{m}_s{}^{out}{}_{t,d,r}$ Mass flow supplied to demand from the hydrogen tank at time t at day d in location r

$E_{t,d,r}^{Acc}$ Energy stored in the battery system at time t at day d in location r

$m_{t,d,r}^{Acc}$ Mass stored in the hydrogen tanks at time t at day d in location r

Coupling renewable power sources with the production of renewable fuel carries over the difficulties of renewable power systems, where the intermittency of these power sources is a relevant design factor. Along these lines, Zhang et al. [11] integrated HRES into the planning and scheduling of renewable-based fuels and power production, identifying bottlenecks and synergies when RE sources are considered; Corengia and Torres [12] formulated a superstructure optimization model that considers the selection of energy sources, type of electrolyzer, its capacity and energy storage devices to select the optimal green hydrogen production capacity for a given renewable energy generation pattern; and Cooper et al. [13] proposed a hydrogen hub designed to operate at variable operation through a bi-level optimization approach.

1.2. State of the art: resilience in power systems

Resilience can be understood as the capacity to withstand misfortune and recover from undesirable events. Applied to any specific field, such as energy systems, infrastructure, material science, and others, this definition needs to be more specific to propose a resilience indicator. This specificity depends on the system under study. The most common approach to define resilience in an energy system is through the systems *health-overtime-curve*, representing the transient state of specific properties over time after an incident that disrupts a stable condition. As discussed in Gasser et al. [14], multiple resilience definitions and measures are defined through this curve. They can be clustered in two groups: *draw-down*, which represents the system's loss due to an undesired event, and *draw-up*, as the system's ability to recover from said adverse event. Some examples of the draw-down section of the curve are:

- **Robustness:** which refers to a system's capacity to withstand a given level of stress or demand without any loss of function ([15]).
- **Absorptiveness:** defined as the degree to which a system can absorb the impacts of a perturbation and minimize consequences with minimal effort ([16]).
- **Resistance:** which refers to the capacity of the system to stay within acceptable ranges of functionality after a negative event ([17]).

The draw-up section of the curve is associated with recovery behaviors. Some examples are:

- **Recovery:** refers to the capacity to recover quickly and at low cost from potentially disruptive events ([17, 18]).
- **Adaptability:** refers to how the system adapts to the newly introduced conditions ([19]).
- **Rebuildability:** refers to the capacity to rebuild all the functions and establish normal operation ([20]).

An innovative approach in considering resilience in HRES design is the one in Vera [21]. Here, a novel resilience indicator that considers a system's capacity to recover from catastrophic events, such as earthquakes, is included as an objective function in a MILP optimization framework. Further, the authors conducted a comprehensive review of resilience indicators based on the system's health over time curve.

Another approach is included in Cho et al. [22] where simultaneous consideration of reliability (withstanding component failure), flexibility (feasible operation under uncertain conditions), and resilience (capacity to withstand catastrophic events) in power systems planning stem as a requirement for future advanced optimization.

1.3. Aim of this study

Most of the resilience metrics described above are based on the system's *health-over-time* curve. Because of this, resilience metrics can be used in dynamic models for planning energy systems. Consequently, the indicators require information on how much system loss occurred at a specific time, how long it lasted, and how fast the system dropped quality and recovered functionality. When design considers long-term planning, such as capacity expansion models, it is not possible to assess with confidence which disruptive events will occur and what their magnitude will be. This results in a research gap when optimizing HRES design with respect to robustness and resilience [5].

This paper introduces a multidimensional design of a regional green hydrogen production system through a novel objective function for HRES operational resilience. This novel resilience metric accounts for the power sources variability, internal physical components failure, and their mitigation through a dual storage system of batteries and H_2 storage. The trade-off between an increased storage capacity, renewable energy variability, plant allocation and the cost of the system is analyzed through a multi-objective optimization of present cost and the proposed operational resilience function through a regional capacity expansion.

We consider Chile as the case study as it is known as one of the countries with a significant capacity to produce clean energy, specifically from solar and wind sources, and has the opportunity to become a global leader in green hydrogen production [23].

2. Problem statement

This work focuses on the allocation and capacity expansion of off-grid green hydrogen production facilities within a delimited geographical region subject to a given hydrogen demand. Each location in the region needs to define whether or not to install renewable energy (RE, solar, or wind) generators, a bank of batteries to store that energy, an electrolyzer, and the associated hydrogen compression stage, and tanks for storage. In addition, we want these designs to be resilient. Figure 1 depicts a representation of the problem.

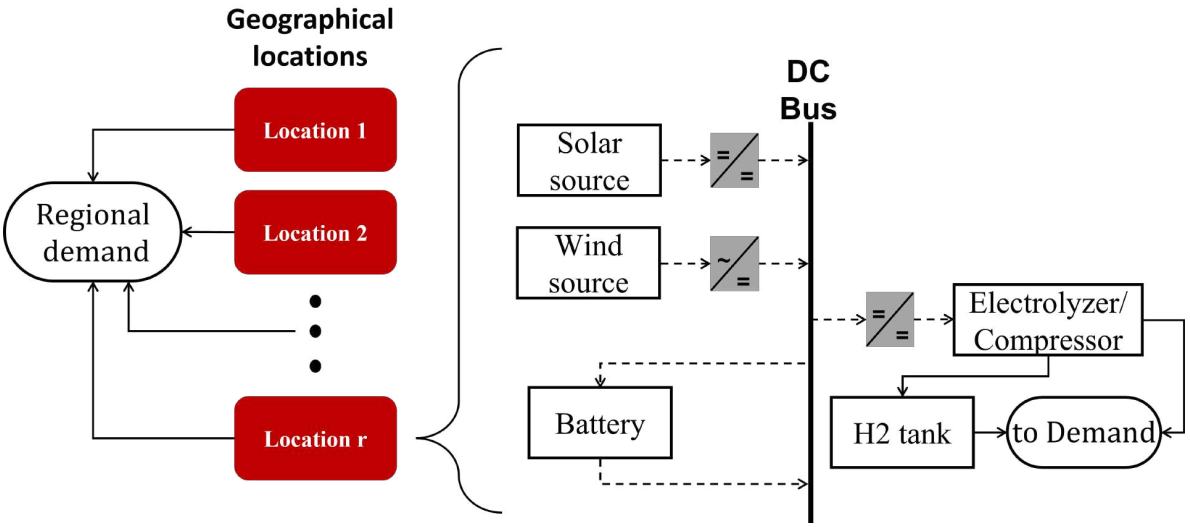

Figure 1: Graphical representation of the regional production problem. A given H_2 demand will be satisfied by r locations; each location needs to define the capacity (solar and wind generators, battery, electrolyzer, storage tanks) to install and their expansion plan for a 15-year time horizon.

Due to the RE sources' intermittency, energy output variability is expected. Said variability may result in a hydrogen production deficit if the system cannot overcome the energy shortfall. Storage capacity, either in batteries or hydrogen tanks, provides the system with flexibility in operation, reducing the effects of an energy deficit but incurring a trade-off of higher capital and operational cost. The main objective of the allocation and subsequent capacity expansion is to determine the optimal sizing and investment plan for each location each year, thriving for an economical and flexible regional hydrogen production system.

The possible processing alternatives can be represented in a superstructure as shown in Fig. 2. In there, mass and energy flows are respectively presented as filled and dashed lines, whereas equipment capacity variables are presented as bold text. The capacity of the equipment can vary in the time horizon. We assume that the plants do not interact with each other.

The superstructure considers that renewable energy sources can directly supply the electrolyzer with power for hydrogen production or feed a battery system to store energy for later discharge to the electrolyzer. Alkaline electrolysis is considered in this study since it is currently the most cost/efficient technology (see Appendix B). Hydrogen is compressed to 30 MPa.

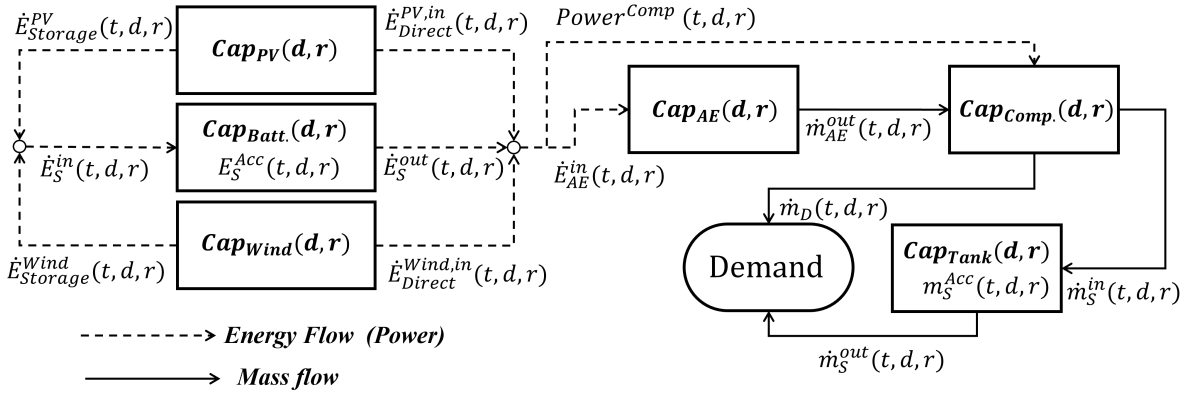

Figure 2: Superstructure for a generic solar/wind green hydrogen production plant. Solar and wind generators can supply power directly to the electrolyzer and compressor; a battery system can be placed to balance intermittencies of the generators. The demand for hydrogen can be directly satisfied from production or from intermediate storage tanks.

Formulation of an optimization problem to solve the superstructure results in a Mixed Integer Linear Programming problem that considers r locations and d days hourly discretized by the index t. A summary of the main equations of the model is given in the following subsections, a complete formulation is available at Appendix C.

3. Modeling

3.1. Representative days approach

The time horizon for design and expansion is considered to be 15 years, from 2025 to 2040. Modeling hourly operations of said systems to capture detailed climatic conditions is known to turn the optimization of the system into an intractable problem [24]. To withstand this complication, a representative days approach is considered. This method is based on selecting specific periods of a historical year; each period is then represented by a characteristic day, which encompasses the overall behavior of the property being analyzed [25]. In this case, said properties are solar radiation and wind speed. Hence, each year is subdivided into three representative days, grouping January to April, May to August, and September to December; then, an hourly subdivision of time is considered for each representative day.

3.2. Equipment

3.2.1. Solar and wind energy generators

Renewable energy sources are modeled according to the installed equipment area in each location on a certain representative day. The variables associated with the installed PV panel area and wind turbine swipe area are $A^{PV}_{d,r}$ and $A^{Wind}_{d,r}$, respectively. The solar energy generation model is presented in Eq. 1, where following [26], the output power is modeled as linearly dependent on the installed area, the solar radiation, and the panel efficiency.

$$\dot{E}^{Direct}_{PV,t,d,r} + \dot{E}^{Storage}_{PV,t,d,r} = \eta_{PV} \cdot {A^{PV}}_{d,r} \cdot {G^{Sun}}_{t,d,r} \tag{1}$$

The wind energy generation model in turbines follows the assumptions in [27] where the total output power depends on the installed swipe area, the capacity factor of the turbine, the average wind speed, and the air density, as shown in Eq. 2.

$$\dot{E}^{Direct}_{Wind,t,d,r} + \dot{E}^{Storage}_{Wind,t,d,r} = \frac{1}{2} \cdot C^{Wind}_{p} \cdot A^{Wind}_{d,r} \cdot \rho_{Air} \cdot (v^{Wind}_{t,d,r})^3 \tag{2}$$

In this study, a constant height of the turbine (80 m) is assumed since an in-depth design of equipment is out of the scope of this study. [28] provides a systematic approach to relate the wind turbine swipe area with the land area requirements; a value of $1.7 \cdot 10^{-3}$ $\left[\frac{m^2 \text{ swipe}}{m^2 \text{ land}}\right]$ is set for the present study.

3.2.2. Energy storage in batteries

Battery systems present two relevant modeling requirements: (i) the energy balance that relates inputs, outputs, and accumulated energy and, (ii) the minimal and maximal states of charge (SOC) required to preserve the battery system's correct operation and lifetime. The energy balance of the battery system is presented in Eq. 3, where charge, discharge, and passive losses are considered.

$${E^{Acc}}_{t,d,r} = \left[1 - L^{Battery}\right] \cdot {E^{Acc}}_{t-1,d,r} + \Delta t \cdot \left(\eta_{Charge} \cdot \dot{E}{s^{in}}_{t-1,d,r} - \frac{\dot{E}{s^{out}}_{t-1,d,r}}{\eta_{Discharge}} \right) \tag{3}$$

A linear constraint for the battery systems' SOC nominal battery capacity constrains the stored energy according to the minimal and maximal SOC as presented in Eq. 4.

$$SOC_{min} \cdot Cap_{Battery,d,r} \leq {E^{Acc}}_{t,d,r} \leq SOC_{max} \cdot Cap_{Battery,d,r} \tag{4}$$

3.2.3. Electrolyzer

We consider an alkaline electrolyzer where the mass of hydrogen produced is related to the power supply as shown in Eq. 5.

$$\dot{E}^{in}_{AE}{}_{t,d,r} = \frac{\dot{m}^{out}_{AE}{}_{t,d,r} \cdot \Delta H}{\eta_{AE}} \tag{5}$$

Here, η_{AE} is the electrolyzer's power to hydrogen efficiency and ΔH the water to hydrogen reaction enthalpy. Following [29, 30], the $\frac{\Delta H}{\eta_{AE}}$ factor is assumed to be 57.3 kWh/kg for alkaline electrolysis.

An essential characteristic of AE technologies is that at small/medium capacities, a minimum load factor is required to avoid persistent shutdown periods in the electrolyzer operation. These shutdown periods can be considered in the optimization problem through binary variables [12]. However, since this study deals with large-scale hydrogen production, the number of required stacks is sufficient to render the minimum load factor negligible. Thus individually accounting for on-off periods is not required.

3.2.4. Compressor

Hydrogen compression is considered as a classical polytropic compression as shown in Eq. 6 [31].

$$P^{Comp} = \frac{\dot{m}^{in}_{Comp} \cdot RkT}{MW \cdot (k-1) \cdot \eta_{Comp}} \left(\left(\frac{P_{H_2}}{P_{el}} \right)^{\frac{k-1}{k}} - 1 \right) \tag{6}$$

In here, the compressor power requirement is dependent on the hydrogen mass flow ($\dot{m}^{in}_{Comp}$), the compressor efficiency (η_{Comp}), the polytropic coefficient (k), the molecular weight of hydrogen (MW), and the ratio of out/in pressure ($\frac{P_{H_2}}{P_{el}}$) inside the vessel. To allow for a linear equation to represent the compression stage, the pressure inside the vessel is considered constant and equal to the maximum pressure of the vessel; then Eq. 6 simplifies to Eq. 7.

$$Power^{Comp}_{t,d,r} = k_{Compressor} \cdot \dot{m}^{out}_{AEt,d,r} \tag{7}$$

where $k_{Compressor}$ brings together all the constant parameters in Eq. 6; following [12] $k_{Compressor}$ is set to 4 $[\frac{kWh}{kg\ H_2}]$.

3.2.5. Hydrogen storage in tanks

Analogous to energy storage in batteries, modeling hydrogen storage in tanks requires two equations: (i) mass balance to relate the level of storage as shown in Eq. 8, where a discharge efficiency of 95% is considered to account for pumping or leakage losses [32], and (ii) the maximum hydrogen level (HL) in the tank as a safety measure which is captured in Eq. 9; a value of 95% of the nominal capacity is considered in this study.

$$m^{Acc}{}_{t,d,r} = m^{Acc}{}_{t-1,d,r} + \Delta t \cdot \left(\dot{m}s^{in}_{t-1,d,r} - \frac{\dot{m}s^{out}_{t-1,d,r}}{\eta_{Tank}} \right) \tag{8}$$

$$0 \leq m^{Acc}{}_{t,d,r} \leq HTL_{max} \cdot Cap_{Tank,d,r} \tag{9}$$

3.3. Capacity expansion modeling

In this problem, any location is allowed to increase or decrease the installed capacity. We consider that any expansion project requires a year-long development and that increments in capacity become available gradually at each trimester. A reduction in capacity is considered to take one trimester. Equation 10 presents the model for technology capacity through the time horizon as a stock constraint.

$$Cap_{i,d,r} = Cap_{i,d-1,r} + \sum_{\hat{d}=d}^{d+2} \left(\frac{1}{3} CapE_{i,\hat{d}} \right) - CapD_{i,d-2,r} \tag{10}$$

In here $\sum_{\hat{d}=d}^{d+2} \left(\frac{1}{3} CapE_{i,\hat{d}} \right)$ corresponds to the gradual increment in capacity in a trimester.

The system's capacity expansion and capacity reduction are respectively associated with binary variables $Y_{i,r,d}$ $X_{i,r,d}$ defined as:

$Y_{i,r,d} = 1$ $\quad$ i starts a capacity expansion at day d in location r

$X_{i,r,d} = 1$ $\quad$ i starts a capacity reduction at day d in location r

If an expansion project is being developed for a technology at a specific location, no other expansion or reduction project can be started for said technology at that location. These logical relations are presented in Eq. 11 (no simultaneous start of expansion and reduction projects); Eq. 12 (no further expansions if an expansion is undergoing) and Eq. 13 (no reduction if expansion project is undergoing).

$$Y_{i,d,r} + X_{i,d,r} \leq 1 \tag{11}$$

$$\sum_{\hat{d}=d+1}^{d+2} Y_{i,\hat{d},r} \leq 2 \cdot (1 - Y_{i,d,r}) \tag{12}$$

$$\sum_{\hat{d}=d+1}^{d+2} X_{i,\hat{d},r} \leq 2 \cdot (1 - Y_{i,d,r}) \tag{13}$$

Upper-bound constraints are implemented to associate the existence of capacity-altering projects with the corresponding magnitude of capacity expansion/ reduction. Equations 14 and 15 show said constraints.

$$CapE_{i,d,r} \leq Max_i \cdot Y_{i,d,r} \tag{14}$$

$$CapD_{i,d,r} \leq Max_i \cdot X_{i,d,r} \tag{15}$$

3.4. Objective functions

3.4.1. Economic objective function

The economic objective function is presented in Eq. 16. Land acquisition, CAPEX, OPEX, H_2 opportunity cost, and a discount factor are considered for each region and are defined below.

$$\text{min: } Land + \sum_{d \in D} DF_d \cdot (CAPEX_d + OPEX_d + {C^{H_2}}_{Op_d}) \tag{16}$$

Land investment. We assume that the land is acquired during the first year for each location and that the total cost is linearly dependent on the purchased area as stated in Eq. 17.

$$Land = \sum_{r \in R} {C_r}^{Area} \cdot A_r \tag{17}$$

CAPEX. Equations 18 and 19 respectively present the capital expenses at the beginning of the time horizon (day 0) and those of subsequent capacity expansions. CAPEX includes the costs of equipment and installation of each technology, where said cost is expressed as $\frac{\text{USD}}{\text{kW, kg/h, kg or kWh}}$ depending on the equipment.

$$CAPEX_0 = \sum_{i \in I,\, r \in R} {C_i}^{Impl} \cdot Cap_{i,0,r} \tag{18}$$

$$CAPEX_{d \neq 0} = \sum_{i \in I,\, r \in R} {C_i}^{Impl} \cdot CapE_{i,d,r} \tag{19}$$

OPEX. OPEX is defined as operational and maintenance cost (O&M) and is considered a percentage of installed capacity (CAPEX); it is calculated as shown in Eq. 20.

$$OPEX_d = \sum_{i \in I,\, r \in R} {C_i}^{Op} \cdot {C_i}^{Impl} \cdot Cap_{i,d,r} \tag{20}$$

In here, the parameter ${C_i}^{Op}$ corresponds to the O&M costs of each trimester associated with the installed capacity.

H_2 opportunity cost. In this study, we refer to H_2 opportunity cost as the loss of potential income related to the decision of storing H_2 instead of selling it to the market. Including this opportunity cost prevents the system to increase resilience by over-storing H_2. We model this opportunity cost as shown in Eq. 21.

$${C^{Op}_{H_2}}_d = P^{Sale}_{H_2} \cdot \sum_{t \in T,\, r \in R} m^{Acc}_{t,d,r} \tag{21}$$

It is important to note that stored energy does not have an opportunity cost since the proposed plants are assumed to be off-grid, and hence, it is not possible to directly sell the stored energy.

Discount factor. A discount factor is considered for the CAPEX, OPEX, and H_2 opportunity cost to account for the time value of money. Equation 22 exhibits the discount factor for a given interest rate r.

$$DF_d = \frac{1}{(1+r)^d} \tag{22}$$

The discount factor of the last representative day is modified as shown in Eq. 23. Here a perpetuity is considered for any capacity still in place at the end of the time horizon. This perpetuity ensures that capacity spikes will not occur near the end of the time horizon due to less relevant present cost values [33].

$$DF_{d_f} = \frac{1}{(1+r)^{d_f}} + \frac{1}{(1+r)^{d_f+1}} \cdot \frac{1}{\left(1 - \frac{1}{(1+r)}\right)} \tag{23}$$

3.4.2. Resilience objective function

In this study, a system will be considered operationally resilient if it has sufficient autonomy to withstand non-catastrophic unfortunate events. Such events are variations of RE sources (exogenous) and internal plant operation failure (endogenous). Both of these events could cause a deficit in hydrogen production, either by a shortage of energy or the unavailability of operational capacity. We will use the term heteronomy to refer to the lack of autonomy of the system due to its dependence on conditions that the system cannot manage.

We consider two essential distinctions of unfortunate events that an autonomous system must endure: (i) *external events* associated with the intrinsic unpredictable behavior that REs have and its effect on the operation of a plant designed through statistical averages of representative days, and (ii) *internal events*, associated with specific failures in the normal plant operation and its corresponding negative effect in production.

Modeling external variability. The model must acknowledge that the parameters of solar radiation and wind speed, used for the sizing of generators of renewable electricity, are averages and are subject to variation. In this sense, locations with a favorable average solar radiation or wind speed might have a high variance, which is not a desired attribute for an off-grid hydrogen plant. This variability is dependent on the installed area of renewable sources at each location, the day and hour of said day, as shown in Eqs. 24 and 25.

$$\dot{Var}_{PV,t,d,r} = \eta_{PV} \cdot {A^{PV}}_{d,r} \cdot \sigma_{PV,t,d,r} \tag{24}$$

$$\dot{Var}_{Wind,t,d,r} = \frac{1}{2} \cdot Cp_{Wind} \cdot {A^{Wind}}_{d,r} \cdot \rho_{Air} \cdot (\sigma_{Wind,t,d,r})^3 \tag{25}$$

Here, $\sigma_{PV,t,d,r}$ and $\sigma_{Wind,t,d,r}$ correspond to the historical deviation of solar radiation and wind speed in an hourly basis for each trimester and each location. The overall variability ${}^{ext}\delta {E^-}_{t,d,r}$ is the sum of both sources

$${}^{ext}\delta {E^-}_{t,d,r} = \sum_{e \in RE} \cdot \dot{Var}_{e,t,d,r} \tag{26}$$

A deficit of energy from renewable sources ultimately results in a deficit in hydrogen production since not all the required power will be supplied to the electrolyzer. The system can compensate for this deficit with storage which can either be in the form of energy in the battery system ([kWh]), which will supply power to the electrolyzer, or as hydrogen itself in tanks ([kg]). The availability of storage can then be calculated as shown in Eq. 27 where:

$$Storage_{t,d,r} = \eta_{Discharge} \cdot {E^{Acc}}_{t,d,r} + \frac{{m^{Acc}}_{t,d,r}}{\eta_{AE}} \tag{27}$$

The net deficit in production due to external variance is then defined as the difference between the expected RE source-induced variability and the compensation that might be achieved by the storage systems. Equation 28 shows the mathematical representation of said term.

$${}^{ext}\Delta {E^-}_{t,d,r} = {}^{ext}\ \delta {E^-}_{t,d,r} - Storage_{t,d,r} \tag{28}$$

Note that if the net externally induced variability ${}^{ext}\Delta {E^-}_{t,d,r}$ is greater than zero, then, the system does not have sufficient storage to withstand the variance of the renewable sources.

Modeling internal variability. According to [34], one of the equipments most prone to fail in a power system are converters, including DC boosters and rectifiers. Figure 1 exhibits where said converters are located in the architecture of the plant's electrical system. Internal variability will consider the availability of renewable sources and the electrolyzer based on their associated converters. Since the availability parameter will vary with the converters circuit architecture [34], this study will refer to accepted literature values for solar PV panels and wind turbines of 96% [35]. DC boosters for alkaline electrolysis circuit designs are still being developed [36], and a 90% availability is assumed.

As shown in Fig. 1, failure in the renewable sources generators will result in a deficit of energy (δE^-). Meanwhile, failure in the electrolyzer will result in a deficit in the associated flow of hydrogen (δM^-). Equations 29 and 30 respectively characterize said energy and mass deficit as a function of the installed capacity ($Cap_{i,d,r}$):

$${}^{int}\delta {E^-}_{d,r} = \sum_{e \in RE} (1 - \Lambda_e) \cdot Cap_{e,d,r} \tag{29}$$

$${}^{int}\delta {M^-}_{d,r} = (1 - \Lambda_{AE}) \cdot Cap_{AE,d,r} \tag{30}$$

where Λ_e and Λ_{AE} represent the availability coefficient of the renewable sources and the alkaline electrolyzer, respectively.

As stated in Section 3.4.2, the storage system may compensate for said variability. In this case, the battery system can only compensate if the failure is in the RE generators (Eq. 31), while a failure in the electrolyzer can only be compensated by storage of hydrogen in tanks (Eq. 32).

$${}^{int}\Delta {E^-}_{t,d,r} = {}^{int}\ \delta {E^-}_{d,r} - \eta_{Disch} \cdot {E^{Acc}}_{t,d,r} \tag{31}$$

$${}^{int}\Delta {M^-}_{t,d,r} = {}^{int}\ \delta {M^-}_{d,r} - {m^{Acc}}_{t,d,r} \tag{32}$$

Proposed objective function for resilience. The objective function for minimizing the net variability in the system is defined as the combination of the equations discussed above. Hence:

$$f_{heteronomy} = \sum_{t,d,r} \eta_{AE} \cdot ({}^{int}\Delta E^{-}{}_{t,d,r} + {}^{ext}\Delta E^{-}{}_{t,d,r}) + {}^{int}\Delta M^{-}{}_{t,d,r} \tag{33}$$

This expression can be interpreted as the systems heteronomy since its value will determine if the design can overcome the external and internal variance with its storage capacity. A negative value indicates that storage is sufficient, and a positive one indicates that storage can't adequately overcome the failures. In this sense, an optimally resilient system can be defined as one with minimal heteronomy.

4. Case study

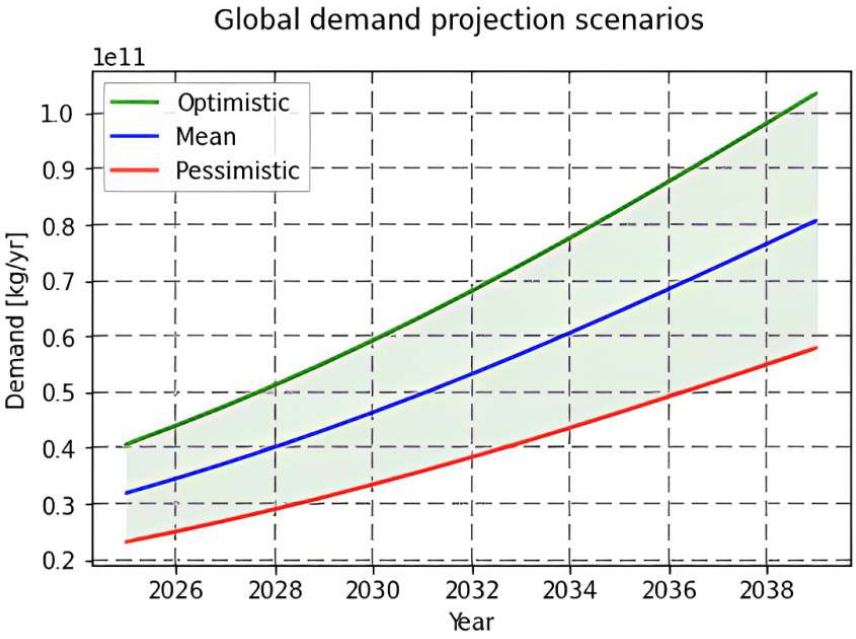

Figure 3: Global hydrogen demand projection through a learning curve for pessimistic, normal, and optimistic scenarios.

We evaluate the production of green hydrogen in five locations of the Biobío region in Chile, namely: Negrete, Aguapie, Lavapie, Rumena, and Colhue. The Biobío region presents favorable sun radiation and wind speed; the mentioned locations are chosen based on data availability in terms of area and climatic conditions data availability. Specific data were obtained from the Chilean wind [37] and solar observatories [38].

In terms of demand, this study will consider the work by Lane et al. (2021) [39], which forecasts the demand for renewable hydrogen at a global scale using Monte Carlo simulations to incorporate uncertainty and a learning curve. Providing the demand scenarios shown in Figure 3. To assess the model, we further assume that Chile plans to supply 20% of the global hydrogen demand and the Biobio region 1% of the total Chilean production. This provides a feasible regional demand for the case study, involving production in all different locations. Appendix B presents the values for the learning curve extracted from Lane et al. [39], each location cost and available area according to the SII database [40], and the technical parameters associated with the case study optimization.

5. Results

The model for the case study in the previous section was implemented in PyOMO [41, 42] and solved using the Gurobi MILP solver [43] on a regular portable laptop. The model constitutes a total of 82,811 variables, where 2,705 variables are binary, and 80,106 are continuous; related through 50,025 equality and 51,745 inequality constraints. The MIP gap terminal condition is maintained at its default value of 1e-4.

5.1. Single objective solutions and multiplicity analysis

Being a MILP problem, it is possible to achieve the same value of the objective function with different values for the arguments, and due to the MIP gap termination condition, a more thorough search might obtain better solutions. To evaluate the optimal design, successive integer cuts were implemented to obtain 3 alternate solutions. Equation 34 shows the "No good cut" [44], where the variable $z_{i,d,r}$ represents the

Table 1: Optimal value for the objective functions in each single-objective model. Alternate solutions' values are presented as a difference from the optimal solution objective.

	Model	
Solution	Economic [USD]	Heteronomic [kg]
Optimal value	1.5996 E+9	-9.4439 E+9
Objective value difference (%)		
Alternative #1	0	$\approx$2.8 E^{-5}
Alternative #2	0	$\approx$2.5E^{-5}
Alternative #3	$\approx 2.8E-4$	$\approx 2.2E-5$

expansion ($X_{i,d,r}$) and decrease ($Y_{i,d,r}$) binary choices of section 3.3, B and NB are the set of basic and non-basic solutions respectively.

$$\sum_{i,d,r \in NB} z_{i,d,r} + \sum_{i,d,r \in B} (1 - z_{i,d,r}) \geq 1 \tag{34}$$

Table 1 shows the results for the single-objective models, i.e., those solutions in which the weights for combining the economic and heteronomy objective functions were either zero (purely resilient objective) or one (purely economic objective). The purely economic single-objective model presents 2 alternative solutions with the same value for the objective function. Meanwhile, no equivalent solutions were found for the pure heteronomy single-objective model; three other alternative solutions where found with negligible differences in the value of the objective function. As shown in Appendix A.1, only a difference in the stored hydrogen at the end of the time horizon and in some expansion rates is observed in these cases. For the rest of the discussion, the results labeled as Optimal value in Table 1 are considered.

5.2. Multi-objective solution – Pareto optimal results

Here, the problem was solved to find the Pareto frontier for the economic and heteronomy objective functions via the weighted sum method. A computation time of 4,545 seconds was required to obtain the multi-objective Pareto frontier.

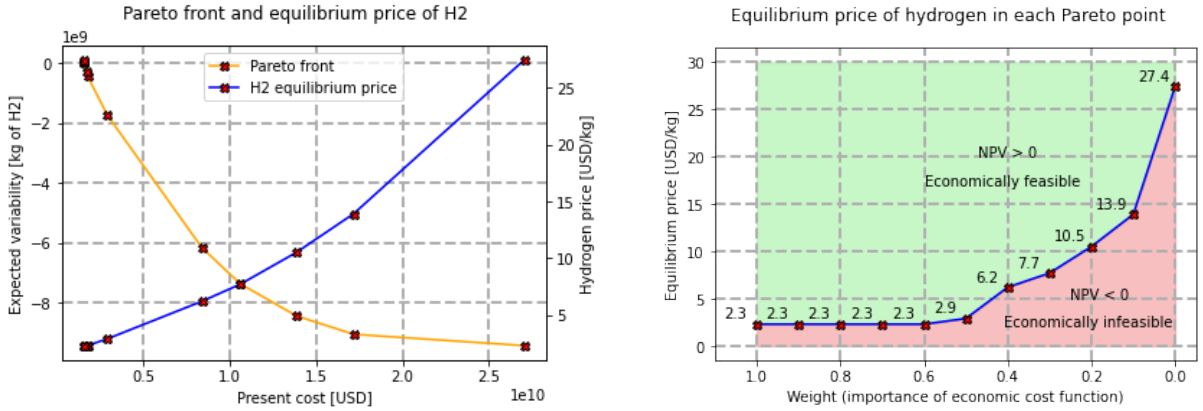

(a) Pareto front and equilibrium price of hydrogen.

(b) Hydrogen equilibrium price for each Pareto point.

Figure 4: Hydrogen equilibrium price for each Pareto point.

Figure 4a exhibits the Pareto curve and the equilibrium price of hydrogen, defined as the one required to achieve a zero Net Present Value (NPV) for the plant investment and production costs. As expected, there is a trade-off between both objective functions, which relates to the fact that designing a more resilient system requires more investment in storage technologies, directly raising the total cost and the equilibrium price for hydrogen. It is important to note that the heteronomy objective function has, at almost all points of the Pareto curve, a negative value. This implies that in almost all solutions the designed network has enough storage to withstand the expected external and internal losses. Figure 4b shows the equilibrium price for hydrogen vs the weight values for each point in the Pareto curve. The green region above the curve corresponds to the hydrogen prices that provide an economically feasible result (positive NPV). Inversely, the red region corresponds to hydrogen prices that make the system economically unfeasible. In the following section, a weight of 0.6, associated with a hydrogen equilibrium price of 2.3 [$\frac{\text{USD}}{\text{kgH}_2}$] is selected as the desired solution from the Pareto frontier, and will be referred as the autonomy enhanced solution. This equilibrium price is lower than the 2.6 [$\frac{\text{USD}}{\text{kg}}\text{H}_2$] benchmark established by the Chilean national hydrogen plan for the Biobío region [45], in addition to presenting a negative heteronomy value. A similar analysis for other weights could be performed if desired.

Table 2: Results overview for the single objective and autonomy enhanced solutions. Capacities are presented as intervals of the minimal and maximum values in the time horizon, expressed as [Min - Max]. Zero values that have an index n referring to the number of years (n) that the capacity value remains at zero. If $n < 1\ year$, no index is implemented.

Result	Model	Rumena	Negrete	Aguapie	Lavapie	Colhue
Starting year	Economic:	2026	2025	2025	2026	2026
	Enhanced:	2026	2025	2025	2026	2026
Solar source capacity [MW]	Economic:	[0 - 14]	[63 - 162]	[0 - 26]	[0 - 22]	[0 - 25]
	Enhanced:	[0 - 16]	[61 - 161]	[0 - 32]	[0 - 24]	[0 - 27]
Wind source capacity [MW]	Economic:	[0 - 109]	[400 - 500]	[44 - 245]	[0 - 167]	[0 - 205]
	Enhanced:	[0 - 109]	[400 - 500]	[44 - 239]	[0 - 161]	[0 - 100]
Battery capacity [MWh]	Economic:	$[0_{(11)} - 2.1]$	0	$[0_{(9)} - 0.8]$	$[0_{(11)} - 4.4]$	0
	Enhanced:	$[0_{(9)} - 5.3]$	[0 - 5.9]	[0 - 4.6]	[0 - 7.7]	[0 - 0.7]
H_2 storage capacity [ton]	Economic:	[0 - 10]	[0 - 50]	[0 - 21]	[0 - 14]	[0 - 16]
	Enhanced:	[1 - 100]	[0 - 100]	[0 - 100]	[0 - 100]	[0 - 100]
H_2 equilibrium price [USD/kg]		Economic			Enhanced	
		$ 2.3			$ 2.3	

5.3. Summary of system design

Table 2 summarizes key changes in the design of HRES systems for green hydrogen production when the economic objective function model is enhanced with the consideration of heteronomy.

Compared to the economic model, no relevant changes in the start years of each location are seen, where Negrete and Aguapie start in 2025 and the rest in 2026. In all cases, a hybrid power system (wind and solar) is selected. Comparing the autonomy enhanced and the economic solution, generation from wind energy sources is implemented at a lower magnitude in Lavapie, Aguapie, and Colhue, followed by an increase in solar capacity for said locations. However, the change is substantial only for Lavapie.

As expected, the most relevant difference between the two objectives relates to storage. Battery storage is not installed at Negrete and Colhue when only the economic function is considered; in contrast, the autonomy enhanced solution increases the energy storage capacity in batteries for each location. Hydrogen storage in tanks also follows the tendency of higher capacities when the heteronomy of the system is considered, increasing to 100 [ton] at each location. It is important to note that the implementation of these storage technologies comes without a noticeable increase in the equilibrium price of hydrogen; for the selected economic/heteronomy combined solution, an investment of 0.37 [USD] is required per kg of H_2 mass variability reduction.

Analyzing the Pareto frontier and how the optimal point shows a considerable increase in present cost, useful remarks arise for future studies: Figure 4a shows that most Pareto points have more than enough mass and energy storage to withstand the accounted variability and that the spike in cost is associated with said increase in storage capacity. Diminishing the value of the upperbound in the constraint associated with storage technologies capacity, specifically mass storage, provides a system design with less idle storage, reducing the overall cost of each point in the Pareto frontier and managing a less considerable cost compared to the economic model. A 75% reduction in the upper bound is analyzed in Appendix A.2 through the Pareto optimal hydrogen equilibrium prices, resulting in an increase in the economically feasible region due to lower equilibrium prices throughout the Pareto front.

5.4. Capacity expansion: single objective and autonomy enhanced solution comparison

In this section, the different system designs are compared for the single objective models and the enhancement of incorporating the multi-objective approach. The capacities of each technology are analyzed for the locations of Negrete and Aguapie, exposing the effects of the proposed heteronomy objective function in the design of the system.

Figure 5 shows the expansion profiles for the economic single objective model in the mentioned regions. In both locations, hydrogen storage and a hybrid power system of solar and wind for the complete time horizon is obtained as the optimal design. In Negrete, the installation of energy sources and hydrogen storage is completed by the first year, and an expansion of the electrolyzer capacity is implemented in the 9th year of operation. Meanwhile, Aguapie completes the installation of hydrogen storage and solar energy

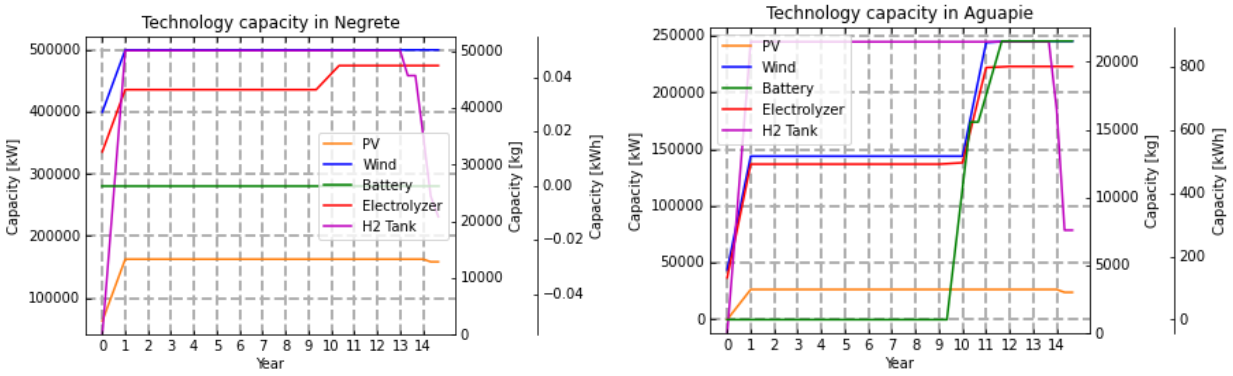

(a) Negrete economic expansion profile

(b) Aguapie economic expansion profile

Figure 5: Expansion profiles of the economic model for Negrete (a) and Aguapie (b) respectively.

generators in the first year of implementation, and an expansion between the 9th and 11th year for the wind energy generators, electrolyzer, and the battery system is considered.

Neither location considers a battery system for the first 9 years of operation, and Negrete does not implement a battery system. The preference for a hydrogen storage system is related to the more cost/efficient hydrogen mass storage over the lithium ion batteries for long periods since the latter have passive losses and present a higher maintenance cost. Because of this, hydrogen storage is preferred over energy storage even when an opportunity cost for hydrogen is implemented.

In both locations, a decrease in the hydrogen storage capacity starts from the 13th year until the end of the time horizon to avoid the perpetuity cost effects (see section 3.4.1), where it is cheaper to diminish hydrogen storage and fulfill demand with production and dispatch the already available stored hydrogen.

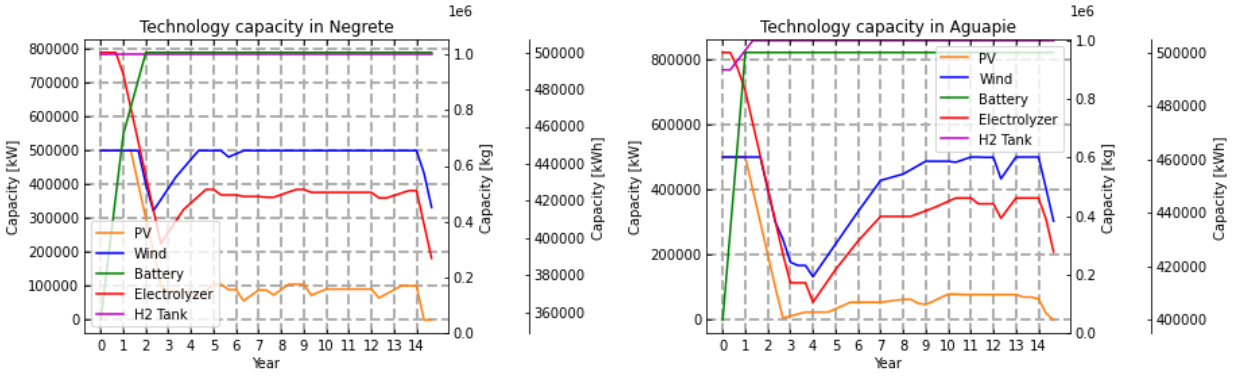

(a) Negrete heteronomic expansion profile

(b) Aguapie heteronomic expansion profile

Figure 6: Expansion profiles of the heteronomy model for Negrete (a) and Aguapie (b) respectively.

Figure 6 shows the expansion profiles for the heteronomy single objective model in Negrete and Aguapie, respectively. Both locations present similar profiles, with the installation of both hydrogen and energy storage systems at maximum capacity for the complete time horizon. A hybrid power system dominated by wind energy is present for each location as well, with a reduction in the generation capacity of the RE sources and electrolyzer until the 3rd and 4th year, when a subsequent expansion is implemented.

The increase of the storage technologies is associated with the objective function formulation in section 3.4.2 as more storage implies a reduced dependence on external and internal variability. The reduction in RE sources generation and electrolyzer capacities seeks to minimize the variability of the system (as defined in sections 3.4.2 and 3.4.2), since a larger installed capacity results in larger internal and external expected variability. Therefore, the heteronomy model maximizes storage capacity while maintaining a minimum required energy source and electrolyzer capacity.

Figure 7 shows the expansion profiles for the autonomy enhanced solution in Negrete and Aguapie, respectively. For both locations, a wind-dominated hybrid power system with dual storage technologies is implemented. In Negrete, the installation of the power generation, the battery system, and the hydrogen storage are complete in the first year of implementation. Aguapie's battery system, hydrogen storage, and power generation from solar energy are fully implemented by the first year, whereas power generation from wind and electrolyzer capacity have an expansion in the 9th year of operation. Both locations present a reduction in capacity in the last 2 years of the time horizon, associated with the perpetuity effects of the economic objective function.

Compared with the purely economic objective, the results show that adding the heteronomy function in a multi-objective approach impacts the system design, promoting dual storage throughout the complete

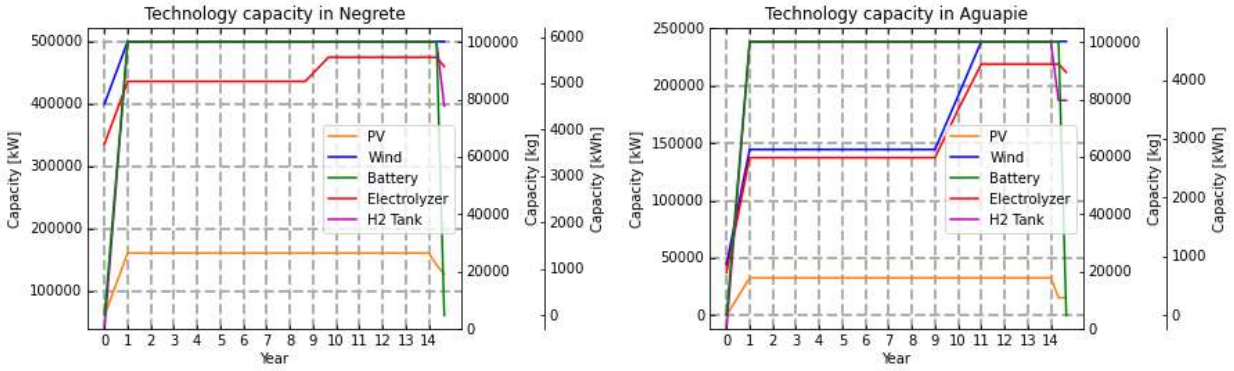

(a) Negrete autonomy enhanced expansion profile

(b) Aguapie autonomy enhanced expansion profile

Figure 7: Expansion profiles of the autonomy enhanced solution for Negrete (a) and Aguapie (b) respectively.

time horizon. The magnitude of the change varies: hydrogen storage increased its maximum value from 50 [ton] in the economic model to 100 [ton] in the autonomy enhanced solution in Negrete and from 21 [ton] to 100 [ton] in Aguapie. Energy storage also increased compared to the economic model, from 800 [kWh] to 4,600 [kWh] in Aguapie, and from 0 [kWh] to 5,900 [kWh] in Negrete. A slight increase in solar power capacity is also perceived in Aguapie.

5.5. Role and effects of hydrogen storage

Figure 8 shows the mass of hydrogen stored in each location throughout the years for the economic, heteronomy, and autonomy enhanced solutions.

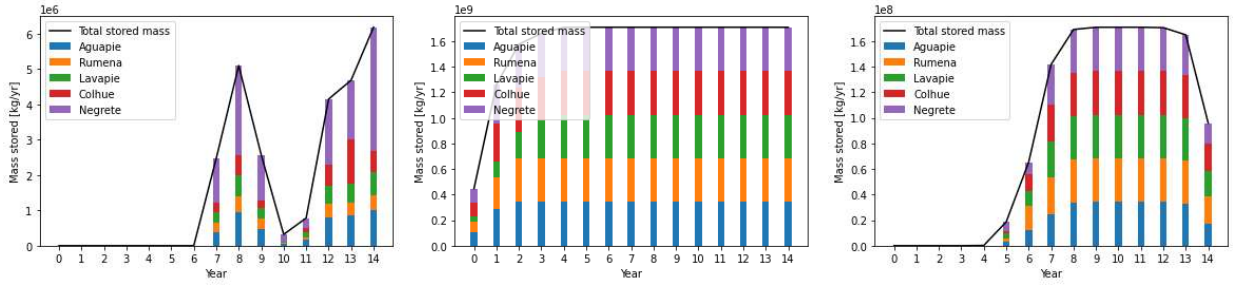

(a) Economic model hydrogen storage profile.

(b) Heteronomy model hydrogen storage profile.

(c) Autonomy enhanced hydrogen storage profile.

Figure 8: Hydrogen storage profile for the single and autonomy enhanced solutions.

As seen, the economic model has a null storage of H_2 mass the first six years, presenting peaks before and after the 10 years of operation. The first peak (8th year) is related to the capacity expansion profiles present in Figures 5a and 5b. The 10th year of the horizon is when most of the system increases its capacity, and since this requires a year to accomplish, the network must have enough storage to fulfill the increase in demand associated with that year beforehand. The second increment after the 10th year relates to the end-of-time effects in the economic objective function since the system stores hydrogen to fulfill demand in the last year of operation. The heteronomy model increases storage rapidly, reaching a constant value by the 3rd year (see Figure 8b) since, as expected, the purely heteronomy-based model maximizes storage to overcome disruptions. The autonomy enhanced solution encompasses the characteristics of both models.

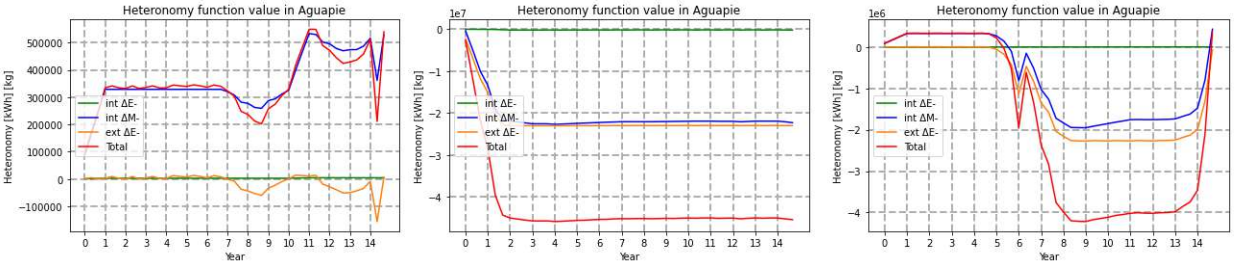

(a) Economic proposed OF profile.

(b) Heteronomic proposed OF profile.

(c) Autonomy enhanced proposed OF profile.

Figure 9: Heteronomy objective function behavior.

The effects of these different storage profiles in the resilience of the system, can be addressed through the value of the heteronomy function since it measures how much autonomy the designed system has. As an example, Fig. 9 exhibits these values for the Aguapie region. Other locations present analogous behaviors.

Figure 9a shows that the total heteronomy value of the economic model design is positive throughout the complete time horizon. This is evidence that the designed system lacks autonomy and would be vulnerable to the exogenous variability of RE sources and endogenous component failure. Hence, the role of storage as a tool for expansion in the economic model doesn't bring operational resilience to the design. In contrast, the autonomy enhanced solution presents a positive value of heteronomy for the first 5 years, and a negative value for the rest of the horizon. This indicates that the multi-objective approach manages to design a storage system that can provide sufficient autonomy to the system for the majority of the time horizon.

The higher installation of storage capacity, the increase of total stored mass, and the objective function behavior shown in Figure 9 shows that, without a relevant increase in the hydrogen equilibrium price, the incorporation of the heteronomy function to the multi-objective optimization manages to design a system that is more autonomous in front of exogenous and endogenous effects than a purely economic model.

6. Conclusion

A multi-objective Mixed Integer Linear Programming model was developed as a decision-making tool to analyze green hydrogen production at a regional level. The tool introduces a novel resilience objective function that minimizes the variability of the system by designing a hybrid storage system capable of mitigating the fluctuations intrinsic to renewable energy sources as well as internal plant failures, striving for simplicity and reasonable computational resources use.

As a case study, the program considers the production of green hydrogen in five regions of Chile that differ in their climate conditions and land cost. In all cases, the optimal resilient system design is a hybrid dual storage system, where wind power is the dominant energy source.

The optimal designs incorporate storage technologies with a capacity larger than the most economical one, covering the estimated deficit in hydrogen and electricity with sufficient surplus throughout most of the time horizon. Considering the five regions, the investment cost of H_2 mass variability reduction is about 0.37 $[\frac{\text{USD}}{\text{kg H}_2}]$ between the purely economically optimal model and the autonomy enhanced one. The hydrogen equilibrium price does not differ much between these two cases, 2.3 [USD/kg], and is lower than the 2.6 [USD/kg] projected by the Chilean hydrogen strategy.

This study's approach can be implemented in other power-to-X technologies for a more diverse regional design, considering the power system's storage/cost trade-off in a manageable manner.

References

[1] A. Olabi, M. A. Abdelkareem, Renewable energy and climate change, Renewable and Sustainable Energy Reviews 158 (2022) 112111. doi:10.1016/j.rser.2022.112111.

[2] D. Maradin, ADVANTAGES AND DISADVANTAGES OF RENEWABLE ENERGY SOURCES UTILIZATION, International Journal of Energy Economics and Policy 11 (2021) 176–183. doi:10.32479/ijeep.11027.

[3] L. M. Swati Negi, Hybrid renewable energy system: A review, International Journal of Electronic and Electrical Engineering (2014).

[4] D. R. Kombargi, D. S. Elborai, D. Y. Anouti, R. Hage, The dawn of green hydrogen, strategy (2021). Revista con proyecciones del mercado de hidrógeno e introducción a su producción.

[5] L. Hammer, E. Veith, Hybrid renewable energy system optimization is lacking consideration of system resilience and robustness: An overview, in: ENERGY 2021, The Eleventh International Conference on Smart Grids, Green Communications and IT Energy-aware Technologies, 2021.

[6] R. Siddaiah, R. Saini, A review on planning, configurations, modeling and optimization techniques of hybrid renewable energy systems for off grid applications, Renewable and Sustainable Energy Reviews 58 (2016) 376–396. doi:10.1016/j.rser.2015.12.281.

[7] C. L. Lara, D. S. Mallapragada, D. J. Papageorgiou, A. Venkatesh, I. E. Grossmann, Deterministic electric power infrastructure planning: Mixed-integer programming model and nested decomposition algorithm, European Journal of Operational Research 271 (2018) 1037–1054. doi:10.1016/j.ejor.2018.05.039.

[8] M. Alraddadi, A. J. Conejo, R. M. Lima, Expansion planning for renewable integration in power system of regions with very high solar irradiation, Journal of Modern Power Systems and Clean Energy 9 (2021) 485–494. doi:10.35833/mpce.2019.000112.

[9] J. Wang, H. Chen, Y. Cao, C. Wang, J. Li, An integrated optimization framework for regional energy planning with a sustainability assessment model, Sustainable Production and Consumption 36 (2023) 526–539. doi:10.1016/j.spc.2022.08.032.

[10] S. Cho, J. Tovar-Facio, I. E. Grossmann, Disjunctive optimization model and algorithm for long-term capacity expansion planning of reliable power generation systems, Computers &amp Chemical Engineering 174 (2023) 108243. doi:10.1016/j.compchemeng.2023.108243.

[11] Q. Zhang, M. Martín, I. E. Grossmann, Integrated design, planning, and scheduling of renewables-based fuels and power production networks, in: Computer Aided Chemical Engineering, Elsevier, 2017, pp. 1879–1884. doi:10.1016/b978-0-444-63965-3.50315-9.

[12] M. Corengia, A. I. Torres, Coupling time varying power sources to production of green-hydrogen: A superstructure based approach for technology selection and optimal design, Chemical Engineering Research and Design 183 (2022) 235–249. doi:10.1016/j.cherd.2022.05.007.

[13] N. Cooper, C. Horend, F. Röben, A. Bardow, N. Shah, A framework for the design &amp operation of a large-scale wind-powered hydrogen electrolyzer hub, International Journal of Hydrogen Energy 47 (2022) 8671–8686. doi:10.1016/j.ijhydene.2021.12.225.

[14] P. Gasser, P. Lustenberger, M. Cinelli, W. Kim, M. Spada, P. Burgherr, S. Hirschberg, B. Stojadinovic, T. Y. Sun, A review on resilience assessment of energy systems, Sustainable and Resilient Infrastructure 6 (2019) 273–299. doi:10.1080/23789689.2019.1610600.
[15] M. Bruneau, S. E. Chang, R. T. Eguchi, G. C. Lee, T. D. O'Rourke, A. M. Reinhorn, M. Shinozuka, K. Tierney, W. A. Wallace, D. von Winterfeldt, A framework to quantitatively assess and enhance the seismic resilience of communities, Earthquake Spectra 19 (2003) 733–752. doi:10.1193/1.1623497.
[16] R. Francis, B. Bekera, A metric and frameworks for resilience analysis of engineered and infrastructure systems, Reliability Engineering &amp System Safety 121 (2014) 90–103. doi:10.1016/j.ress.2013.07.004.
[17] S. Jackson, T. L. J. Ferris, Resilience principles for engineered systems, Systems Engineering 16 (2012) 152–164. doi:10.1002/sys.21228.
[18] Y. Y. Haimes, K. Crowther, B. M. Horowitz, Homeland security preparedness: Balancing protection with resilience in emergent systems, Systems Engineering 11 (2008) 287–308. doi:10.1002/sys.20101.
[19] National Academy of Sciences, Disaster Resilience: A national imperative, The National Academies Press, 2012. doi:10.17226/13457.
[20] H. R. Heinimann, K. Hatfield, Infrastructure resilience assessment, management and governance - state and perspectives, in: NATO Science for Peace and Security Series C: Environmental Security, Springer Netherlands, 2017, pp. 147–187. doi:10.1007/978-94-024-1123-2_5.
[21] G. Vera, Development of a method for planning a resilient multi.vector energy system through a multi-objective optimization model (2020). Optimización y análisis de resiliencia en HREs bajo escenarios catastróficos. Problema lineal y simulación de montecarlo.
[22] S. Cho, C. Li, I. E. Grossmann, Recent advances and challenges in optimization models for expansion planning of power systems and reliability optimization, Computers &amp Chemical Engineering 165 (2022) 107924. doi:10.1016/j.compchemeng.2022.107924.
[23] T. C. e. I. Ministerio de Ciencia, The Chilean Potential for Exporting Renewable Energy, 2021.
[24] P. Nahmmacher, E. Schmid, L. Hirth, B. Knopf, Carpe diem: A novel approach to select representative days for long-term power system modeling, Energy 112 (2016) 430–442. doi:10.1016/j.energy.2016.06.081.
[25] I. J. Scott, P. M. Carvalho, A. Botterud, C. A. Silva, Clustering representative days for power systems generation expansion planning: Capturing the effects of variable renewables and energy storage, Applied Energy 253 (2019) 113603. doi:10.1016/j.apenergy.2019.113603.
[26] A. Molina, F. Martínez, Modelo de generación fotovoltaica, Technical Report, Ministerio de Energía, 2017.
[27] T. Ackermann (Ed.), Wind Power in Power Systems, John Wiley & Sons, Ltd, 2005. doi:10.1002/0470012684.
[28] S. Afsharian, P. A. Taylor, On the potential impact of lake erie wind farms on water temperatures and mixed-layer depths: Some preliminary 1-d modeling using COHERENS, Journal of Geophysical Research: Oceans 124 (2019) 1736–1749. doi:10.1029/2018jc014577.
[29] O. Schmidt, A. Gambhir, I. Staffell, A. Hawkes, J. Nelson, S. Few, Future cost and performance of water electrolysis: An expert elicitation study, International Journal of Hydrogen Energy 42 (2017) 30470–30492. doi:10.1016/j.ijhydene.2017.10.045.
[30] J. Proost, Critical assessment of the production scale required for fossil parity of green electrolytic hydrogen, International Journal of Hydrogen Energy 45 (2020) 17067–17075. doi:10.1016/j.ijhydene.2020.04.259.
[31] M. Martín, Optimal year-round production of DME from CO2 and water using renewable energy, Journal of CO2 Utilization 13 (2016) 105–113. doi:10.1016/j.jcou.2016.01.003.
[32] M. El-Sharkh, M. Tanrioven, A. Rahman, M. Alam, Cost related sensitivity analysis for optimal operation of a grid-parallel PEM fuel cell power plant, Journal of Power Sources 161 (2006) 1198–1207. doi:10.1016/j.jpowsour.2006.06.046.
[33] S. You, S. W. Hadley, M. Shankar, Y. Liu, Co-optimizing generation and transmission expansion with wind power in large-scale power grids—implementation in the US eastern interconnection, Electric Power Systems Research 133 (2016) 209–218. doi:10.1016/j.epsr.2015.12.023.
[34] S. Peyghami, Z. Wang, F. Blaabjerg, A guideline for reliability prediction in power electronic converters, IEEE Transactions on Power Electronics 35 (2020) 10958–10968. doi:10.1109/tpel.2020.2981933.
[35] A. K. Kaviani, G. Riahy, S. Kouhsari, Optimal design of a reliable hydrogen-based stand-alone wind/PV generating system, considering component outages, Renewable Energy 34 (2009) 2380–2390. doi:10.1016/j.renene.2009.03.020.
[36] D. Guilbert, S. M. Collura, A. Scipioni, DC/DC converter topologies for electrolyzers: State-of-the-art and remaining key issues, International Journal of Hydrogen Energy 42 (2017) 23966–23985. doi:10.1016/j.ijhydene.2017.07.174.
[37] Ministerio de Energía - Gobierno de Chile, Explorador solar, Online, 2023. URL: `https://solar.minenergia.cl/inicio`.
[38] Ministerio de Energía - Gobierno de Chile, Explorador eólico, 2023. URL: `https://eolico.minenergia.cl/inicio`.
[39] B. Lane, J. Reed, B. Shaffer, S. Samuelsen, Forecasting renewable hydrogen production technology shares under cost uncertainty, International Journal of Hydrogen Energy 46 (2021) 27293–27306. doi:10.1016/j.ijhydene.2021.06.012.
[40] Servicio de Impuestos Internos (SII), REVALÚO DE SITIOS NO EDIFICADOS, PROPIEDADES ABANDONADAS O POZOS LASTREROS, Technical Report, Servicio de Impuestos Internos, 2021.
[41] M. L. Bynum, G. A. Hackebeil, W. E. Hart, C. D. Laird, B. L. Nicholson, J. D. Siirola, J.-P. Watson, D. L. Woodruff, Pyomo–optimization modeling in python, volume 67, third ed., Springer Science & Business Media, 2021.
[42] W. E. Hart, J.-P. Watson, D. L. Woodruff, Pyomo: modeling and solving mathematical programs in python, Mathematical Programming Computation 3 (2011) 219–260.
[43] Gurobi Optimization, LLC, Gurobi Optimizer Reference Manual, 2023. URL: `https://www.gurobi.com`.
[44] E. Balas, R. Jeroslow, Canonical cuts on the unit hypercube, SIAM Journal on Applied Mathematics 23 (1972) 61–69. doi:10.1137/0123007.
[45] Ministerio de Energía - Gobierno de Chile, ESTRATEGIA NACIONAL DE HIDRÓGENO VERDE, Technical Report, 2020.
[46] P. F., B. A., B. C., Thermal management of solid oxide electrolysis cell systems through air flow regulation, Chemical Engineering Transactions 61 (2017) 1069–1074. doi:10.3303/CET1761176.
[47] A. Christensen, Assessment of Hydrogen Production Costs from Electrolysis: United States and Europe, Technical Report, Three Seas Consulting, 2020.
[48] J. Lorenzo, Rendimiento de placas solares, 2015. URL: `<https://www.sfe-solar.com/>`.
[49] G. Pamparana, W. Kracht, J. Haas, G. Díaz-Ferrán, R. Palma-Behnke, R. Román, Integrating photovoltaic solar energy and a battery energy storage system to operate a semi-autogenous grinding mill, Journal of Cleaner Production 165 (2017) 273–280. doi:10.1016/j.jclepro.2017.07.110.
[50] B. Newman, The spacing of wind turbines in large arrays, Energy Conversion 16 (1977) 169–171. doi:10.1016/0013-7480(77)90024-9.
[51] Y. Cengel, Thermodynamics: An Engineering Approach 5th edition, 2005.
[52] H. Yang, L. Lu, W. Zhou, A novel optimization sizing model for hybrid solar-wind power generation system, Solar Energy 81 (2007) 76–84. doi:10.1016/j.solener.2006.06.010.

[53] CNE, Fijación de presios de nuco corto, Technical Report, Comisión Nacional de Energía, 2022.
[54] LAZARD, Lazard's levelized cost of energy analysis - version 15.0, 2021. URL: <https://www.lazard.com>.
[55] C. W, A. Frazier, NREL: technical Report: Cost Projections for Utility-Scale Battery Storage, Technical Report, National Renewable Energy Laboratory (NREL), 2019.
[56] G. Parks, R. Boyd, J. Cornish, R. Remick, Hydrogen Station Compression, Storage, and Dispesing Technical Status and Costs: Systems Integration, Technical Report, National Renewable Energy Laboratory (NREL), 2014.
[57] U. E. I. Administration, Cost and Performance Characteristics of New Generating Technologies, Technical Report, U.S. Energy Information Administration, 2021.
[58] J. Yates, R. Daiyan, R. Patterson, R. Egan, R. Amal, A. Ho-Baille, N. L. Chang, Techno-economic analysis of hydrogen electrolysis from off-grid stand-alone photovoltaics incorporating uncertainty analysis, Cell Reports Physical Science 1 (2020) 100209. doi:10.1016/j.xcrp.2020.100209.
[59] N. R. E. L. (NREL), Hydrogen Station Compression,Storage, and DispensingTechnical Status and Costs, Technical Report, NREL, 2014.
[60] B. Dursun, E. Aykut, An investigation on wind/PV/fuel cell/battery hybrid renewable energy system for nursing home in istanbul, Proceedings of the Institution of Mechanical Engineers, Part A: Journal of Power and Energy 233 (2019) 616–625. doi:10.1177/0957650919840519.

Appendix A. Complementary results

Appendix A.1. Alternative designs

Figure A.10 shows an example of the design variations found through the integer cuts for Aguapie.

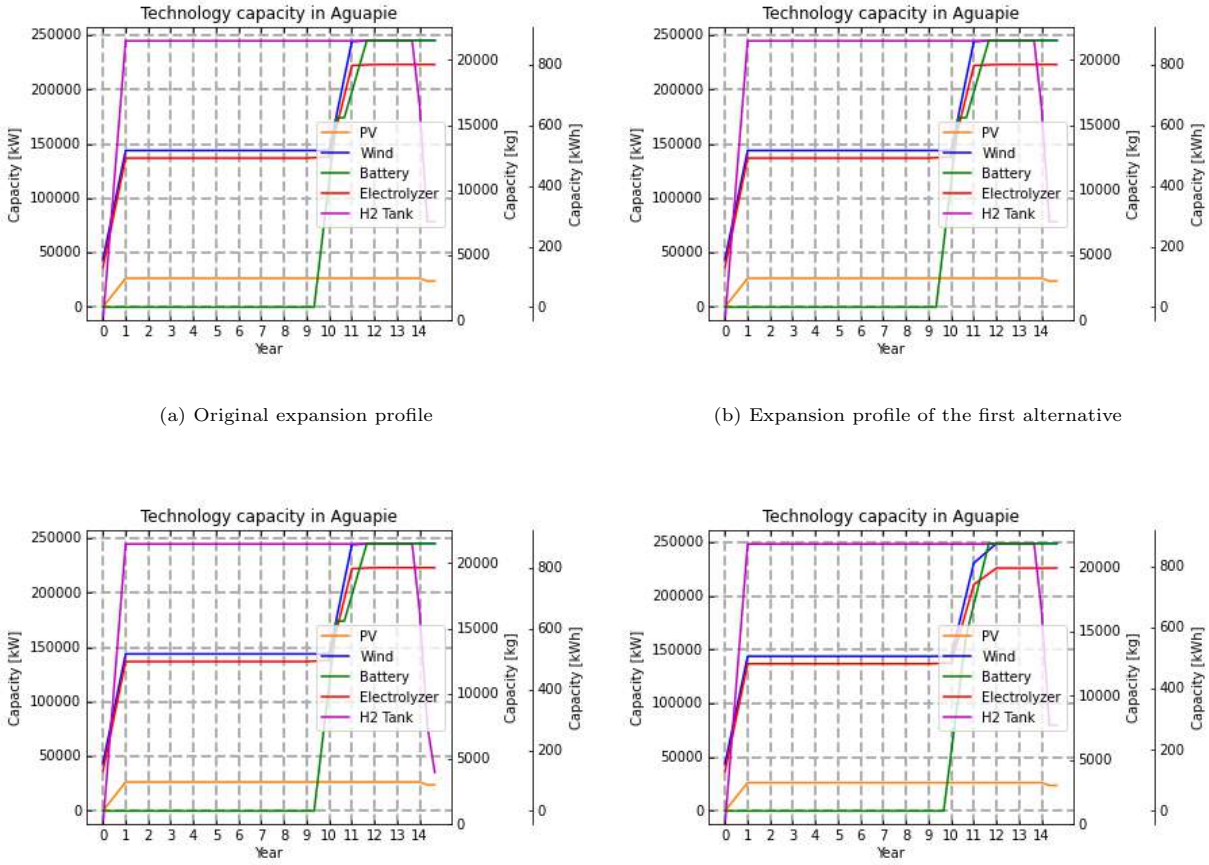

(a) Original expansion profile

(b) Expansion profile of the first alternative

(c) Expansion profile of the second alternative

(d) Expansion profile of the third alternative

Figure A.10: Alternative designs for the Aguapie expansion. Obtained through the "No good" integer cut.

Only slight variations of design can be seen for the final hydrogen storage capacity, where the alternative of Figure A.10c decreases capacity more than the other solutions. Another difference can be seen for the profile of the third alternative design in Figure A.10d, where the expansion of the 9th year is delayed one trimester, incurring in a step-wise increase before the maximum capacities for wind turbines, electrolyzer and battery storage is achieved. None of the found solutions differ from each other considerably, neither in the magnitude of the installed capacities or in the overall profile for the system expansion.

Appendix A.2. Storage capacity constraint effect in price

The effect of reducing the M constant in equation C.1 for the mass storage tank influences the Pareto optimal solutions since the heteronomic model will have a smaller storage capacity upper bound and in consequence a different objective function value. The effect of a 75% reduction in the upperbound is depicted by Figure A.11.

The reduction provided a greater economically feasible region due to the lower prices in the Pareto frontier. In consequence, said parameter must be chosen carefully to avoid overestimating the maximum storage capacity of the desired system.

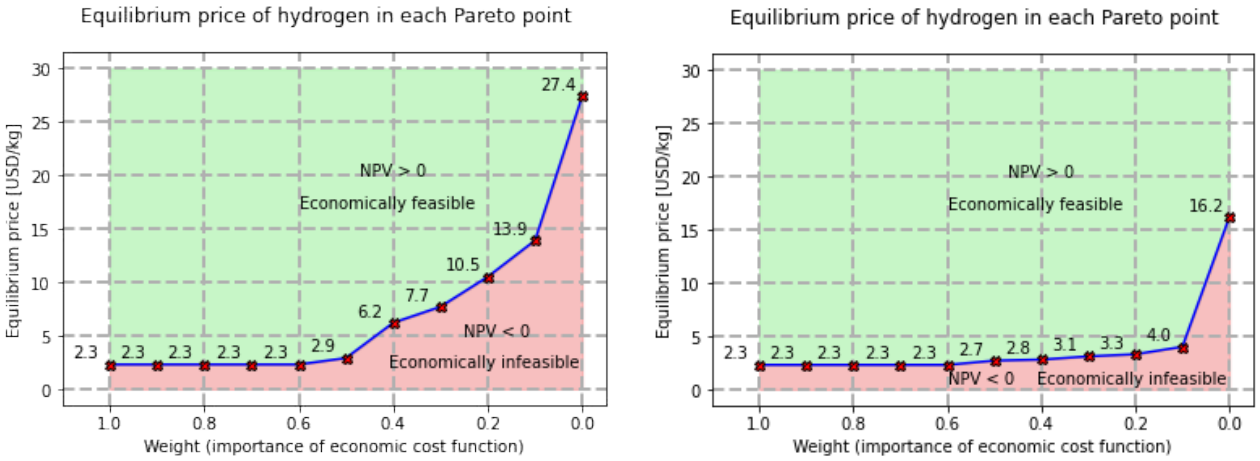

(a) M constant associated with mass storage is set to 10^6

(b) M constant associated with mass storage is set to $2.5 \cdot 10^5$

Figure A.11: Equilibrium price of hydrogen in each Pareto optimal solution.

Appendix B. Parameters for the case study

Appendix B.1. Hydrogen demand projection

The global hydrogen demand behavior is modeled as a learning curve according to equation B.1.

$$D_t = \frac{D_f}{1 + e^{-k \cdot (t - t_0)}} + D_0 \tag{B.1}$$

Where D_t is the global hydrogen demand at time t, D_F is the final market production, D_0 is the initial market production, k is the growth factor and t_0 is the initial year of evaluation.

Table B.3: Parameters for the demand projection through a learning curve behavior.

Parameter	Value	Unit	Reference
Initial market	Mean: $1.5 \cdot 10^9$ SD: 0	$[kg/yr]$ $[kg/yr]$	[39]
Final market	Mean: $1.66 \cdot 10^{11}$ SD: $2.4 \cdot 10^{10}$	$[kg/yr]$ $[kg/yr]$	[39]
Growth	0.1	[-]	[39]
Shift	4.5	[-]	[39]
Biobio global market share	0.1%	[-]	Assumed

Appendix B.2. Electrolysis technologies cost comparison

Schmidt et al. [29] and Proost [30] provide the $\frac{\Delta H}{\eta_{Electr.}}$ parameter for alkaine electrolysis (AE) and proton exchange memmbrane electrolysis (PEME), meanwhile F. et al. [46] reports the value for solid oxide electrolysis (SOE). The levelized cost of each technology is reported by Christensen [47]. With the levelized cost and efficiency, the cost of mass production can be calculated as depicted in equation B.2.

$$Cost^{Mass}_{Electr.} = C^{Impl}_{Electr.} \cdot \Delta H / \eta_{Electr.} \tag{B.2}$$

Equations B.3, B.4, and B.5 show the cost for each electrolyzer technology.

$$\begin{aligned} Cost^{Mass}_{AE} &= 1,083 \left[\frac{USD}{kW}\right] \cdot 53.7 \left[\frac{kW}{kg/h}\right] \\ &\approx 58,157 \left[\frac{USD}{kg/h}\right] \end{aligned} \tag{B.3}$$

$$\begin{aligned} Cost^{Mass}_{PEME} &= 1,182 \left[\frac{USD}{kW}\right] \cdot 53.7 \left[\frac{kW}{kg/h}\right] \\ &\approx 63,473 \left[\frac{USD}{kg/h}\right] \end{aligned} \tag{B.4}$$

$$Cost_{SOE}^{Mass} = 2,285 \left[\frac{USD}{kW}\right] \cdot 42.7 \left[\frac{kW}{kg/h}\right]$$
$$\approx 97,570 \left[\frac{USD}{kg/h}\right] \tag{B.5}$$

The AE presents the lower cost of hydrogen production according to the parameters that the formulated model uses. Since no difference in availability can be factually stablished, the economic part of the multi-objective function will always choose AE technologies over their counterparts.

Appendix B.3. Parameter values

Table B.4 presents the parameters used for the case study. For non-indexable parameters the value and reference are stated separately. Meanwhile, indexable parameters are presented in groups.

Table B.4: Parameters for the case study

Parameter		Value	Unit	Source
$\frac{\Delta H}{\eta_{AE}}$		53.7	[kWh/kg]	[29], [30]
η_{PV}		20%	[kW_{out}/kW_{in}]	[48]
η_{Charge}		95%	[-]	[49]
$\eta_{Discharge}$		95%	[-]	[49]
η_{Tank}		95%	[-]	Assumed
λ		$1.7 \cdot 10^{-3}$	[m^2 swipe/m^2 Land]	[28][50]
ρ_{Air}		1.26	[kg/m^3]	[51]
C_P^{Wind}		0.4	[-]	[38]
HTL_{Max}		95%	[-]	Assumed
$k_{Compressor}$		4	[kWh/kg]	[12]
$L^{Battery}$		0.02%	[-]	[52]
$P_{H_2}^{Sale}$		2.6	[USD/kg]	[45]
Λ_i	PV	96%	[-]	[35]
	Wind	96%	[-]	[35]
	Electrolyzer	90%	[-]	Assumed
A_r^{Max}	Aguapie	50,000	[ha]	[40]
	Rumena	2,000	[ha]	[40]
	Lavapie	850	[ha]	[40]
	Colhue	41,200	[ha]	[40]
	Negrete	20,000	[ha]	[40]
C_i^{Impl}	PV	970	[USD/kW]	[53]
	Wind	1,350	[USD/kW]	[54]
	Battery	350	[USD/kWh]	[55]
	AE	1,083	[USD/kW]	[47]
	Compressor	250	[USD/(kg/hr)]	[12]
	Tank	1,000	[USD/kg]	[56]
C_i^{Op} (as trimester)	PV	0.55%	[-]	[53]
	Wind	0.6%	[-]	[57]
	Battery	2.5%	[-]	[57]
	AE	0.6%	[-]	[58]
	Compressor	0.24%	[-]	[59]
	Tank	0.24%	[-]	[60]
Max_i	Upgrade/Downgrade	10^5	[-]	-
	PV,Wind,Battery	10^6	[-]	-
	AE, Compressor, Tank	$5{\cdot}10^6$	[-]	-

Appendix C. Condensed model formulation and nomenclature

1. **Sets**
   - Renewable energy sources:
   $$e \in RE = \{PV, Wind\}$$
   - Sized technologies:
   $$i \in I = RE \cup \{AE, Compressor, Battery, Tank\}$$
   - Discrete time of day:
   $$t \in T = \{0, 1, 2, 3, ..., 23\}$$
   - Representative days (trimester) in a 15 year time horizon:
   $$d \in D = \{0, 1, 2, 3, ..., 44\}$$
   - Locations where plants can be installed:
   $$r \in R = \{Aguapie, Rumena, Lavapie, Colhue, Negrete\}$$
2. **Variables**
   - If location r is used in the regional production:
   $$H_r \in \{0, 1\}$$
   - If technology i starts a expansion project at day d in location r:
   $$Y_{i,d,r} \in \{0, 1\}$$
   - If technology i starts a downgrade project at day d in location r:
   $$X_{i,d,r} \in \{0, 1\}$$
   - Amount of capacity expansion/downgrade for project associated with technology i at day d in location r:
   $$CapE_{i,d,r} \;\; CapD_{i,d,r} \in \mathbb{R}^+$$
   - Capacity of technology i at day d in location r:
   $$Cap_{i,d,r} \in \mathbb{R}^+$$
   - Bough Land in location r:
   $$A_r \in \mathbb{R}^+$$
   - Installed area of PV panels and wind turbine swipe area in location r:
   $$A^{PV}{}_{d,r} \; A^{Wind}{}_{d,r} \in \mathbb{R}^+$$
   - Compressor power consumption in time t at day d in location r:
   $$Power^{Comp}{}_{t,d,r} \in \mathbb{R}^+$$
   - Energy flow directed to battery storage in time t at day d in location r:
   $$\dot{E}_s^{in}{}_{t,d,r} \in \mathbb{R}^+$$
   - Energy flow directed to the AE from the battery system in time t at day d in location r:
   $$\dot{E}_s^{out}{}_{t,d,r} \in \mathbb{R}^+$$
   - Energy flow directed to the AE from the energy source e in time t at day d in location r:
   $$\dot{E}^{Direct}_{e,t,d,r} \in \mathbb{R}^+$$

- Energy flow directed to the battery system from the energy source e in time t at day d in location r:

$$\dot{E}^{Storage}_{e,t,d,r} \in \mathbb{R}^{+}$$

- Energy flow supplied to the AE in time t at day d in location r:

$$\dot{E}^{in}_{AE\,t,d,r} \in \mathbb{R}^{+}$$

- Mass flow out from the AE in time t at day d in location r:

$$\dot{m}^{out}_{t,d,r} \in \mathbb{R}^{+}$$

- Mass flow supplied to the hydrogen tank in time t at day d in location r:

$$\dot{m}^{in}_{s\,t,d,r} \in \mathbb{R}^{+}$$

- Mass flow supplied to demand directly from the AE in time t at day d in location r:

$$\dot{m}^{d}_{t,d,r} \in \mathbb{R}^{+}$$

- Mass flow supplied to demand from the hydrogen tank in time t at day d in location r:

$$\dot{m}^{out}_{s\,t,d,r} \in \mathbb{R}^{+}$$

- Energy stored in the battery system in time t at day d in location r:

$$E^{Acc}{}_{t,d,r} \in \mathbb{R}^{+}$$

- Mass stored in the hydrogen tank in time t at day d in location r:

$$m^{Acc}{}_{t,d,r} \in \mathbb{R}^{+}$$

3. **Constraints**

- If the location is not chosen, no capacity is allowed:

$$Cap_{i,d,r} \leq Max_i \cdot H_r \tag{C.1}$$

- Expansion and downgrade projects can't start at the same day for technology i at day d in location r:

$$Y_{i,d,r} + X_{i,d,r} \leq 1 \tag{C.2}$$

- Expansion projects last for a year in implementation. Meanwhile, no expansion or downgrade of the same technology can occur:

$$\sum_{\hat{d}=d+1}^{d+2} Y_{i,\hat{d},r} \leq 2 \cdot (1 - Y_{i,d,r}) \tag{C.3}$$

$$\sum_{\hat{d}=d+1}^{d+2} X_{i,\hat{d},r} \leq 2 \cdot (1 - Y_{i,d,r}) \tag{C.4}$$

- The choice of expansion or downgrade bounds the augmentation or diminution of capacity:

$$CapE_{i,d,r} \leq Max_i \cdot Y_{i,d,r} \tag{C.5}$$

$$CapD_{i,d,r} \leq Max_i \cdot X_{i,d,r} \tag{C.6}$$

- Variation of capacity represented as a stock constraint. The implementation of upgrades is achieved progressively through the year by trimester:

$$Cap_{i,d,r} = Cap_{i,d-1,r} + \sum_{\hat{d}=d}^{d+2} \left(\frac{1}{3} CapE_{i,\hat{d}} \right) - CapD_{i,d-2,r} \tag{C.7}$$

- Total produced solar energy depends on installed area:

$$\dot{E}^{Direct}_{PV,t,d,r} + \dot{E}^{Storage}_{PV,t,d,r} = \eta_{PV} \cdot {A^{PV}}_{d,r} \cdot {G^{Sun}}_{t,d,r} \tag{C.8}$$

- Total produced wind energy depends on installed swipe area:

$$\dot{E}^{Direct}_{Wind,t,d,r} + \dot{E}^{Storage}_{Wind,t,d,r} = \frac{1}{2} Cp_{Wind} \cdot {A^{Wind}}_{d,r} \cdot \rho_{Air} \cdot (v_{Windt,d,r})^3 \tag{C.9}$$

- Renewable energy is bounded by installed capacity:

$$\dot{E}^{Direct}_{e,t,d,r} + \dot{E}^{Storage}_{e,t,d,r} \leq Cap_{e,d,r} \tag{C.10}$$

- Installed area of PV and wind cannot exceed bought Land at each location:

$${A^{PV}}_{d,r} + \frac{{A^{PV}}_{d,r}}{\lambda} \leq A_r \tag{C.11}$$

- Bought Land cannot exceed the maximum available area:

$$A_r \leq H_r \cdot A^{Max}_r \tag{C.12}$$

- The battery system has to operate in between acceptable SOC values to preserve functionality:

$$SOC_{min} \cdot Cap_{Battery,d,r} \leq {E^{Acc}}_{t,d,r} \tag{C.13}$$

$${E^{Acc}}_{t,d,r} \leq SOC_{max} \cdot Cap_{Battery,d,r} \tag{C.14}$$

- Effective mass flow out of the electrolyzer:

$$\frac{\eta_{AE}}{\Delta H} \cdot \dot{E}^{in}_{AEt,d,r} = \dot{m}^{out}_{t,d,r} \tag{C.15}$$

- Maximum capacity for the electrolyzer:

$$\dot{E}^{in}_{AEt,d,r} \leq Cap_{AE,d,r} \tag{C.16}$$

- Compressors capacity restricts outgoing mass flow:

$$\dot{m}^{d}_{t,d,r} + {\dot{m}^{out}_{s}}_{t,d,r} \leq Cap_{Compressor,d,r} \tag{C.17}$$

- Compressor power consumption according to mass flow:

$$Power^{Comp}_{t,d,r} = k_{Compressor} \cdot \dot{m}^{out}_{AEt,d,r} \tag{C.18}$$

- Mass storage must respect a maximal hydrogen level as a safety measure:

$$0 \leq {m^{Acc}}_{t,d,r} \leq HTL_{max} \cdot Cap_{Tank,d,r} \tag{C.19}$$

- Energy balance for the battery system:

$${E^{Acc}}_{t,d,r} = \left[1 - L^{Battery}\right] \cdot {E^{Acc}}_{t-1,d,r} + \Delta t \cdot \left(\eta_{Charge} \cdot {\dot{E}s^{in}}_{t-1,d,r} - \frac{{\dot{E}s^{out}}_{t-1,d,r}}{\eta_{Discharge}} \right) \tag{C.20}$$

- Energy balance for total energy entering the battery system:

$$\sum_{e \in RE} \dot{E}^{Storage}_{e,t,d,r} = {\dot{E}s^{in}}_{t,d,r} \tag{C.21}$$

- Energy balance for total energy entering the electrolyzer:

$$\sum_{e \in RE} \dot{E}^{Direct}_{e,t,d,r} + {\dot{E}s^{in}}_{t,d,r} = \dot{E}^{in}_{AEt,d,r} + Power^{Comp}_{t,d,r} \tag{C.22}$$

- Compressor mass balance:

$$\dot{m}^{out}_{AEt,d,r} = \dot{m}^{d}_{t,d,r} + {\dot{m}^{in}_{s}}_{t,d,r} \tag{C.23}$$

- Hydrogen storage mass balance:

$$m^{Acc}{}_{t,d,r} = m^{Acc}{}_{t-1,d,r} + \Delta t \cdot \left(\dot{m}s^{in}_{t-1,d,r} - \frac{\dot{m}s^{out}_{t-1,d,r}}{\eta_{Tank}} \right) \tag{C.24}$$

- Demand is associated to a complete trimester by the d index. Considering that a trimester contains 120 representative days the demand fulfilment is characterized as:

$$120 \cdot \left(\sum_{t \in T} \sum_{r \in R} \dot{m}_s^{out}{}_{t,d,r} + \dot{m}^s_{t,d,r} \right) = Demand_d \tag{C.25}$$

4. **Objective functions**

- Minimize present cost:

$$\text{Min: } Land + \sum_{d \in D} DF_d \cdot (CAPEX_d + OPEX_d + C^{H_2}{}_{Op_d}) \tag{C.26}$$

- Minimize heteronomy:

$$\text{Min: } {}^{int}\Delta M^-{}_{t,d,r} + \eta_{AE} \cdot ({}^{int}\Delta E^-{}_{t,d,r} + {}^{ext}\Delta E^-{}_{t,d,r}) \tag{C.27}$$